Simultaneous Calibration of Anomalous Electron Collision Frequency and Anomalous Electron Heating in a Hall Thruster Simulation

IEPC-2025-202

Presented at the 39th International Electric Propulsion Conference
Imperial College London • London, United Kingdom
14-19 September 2025

Julian Lopez-Uricoechea[1], Dan Lev[2], Mitchell L. R. Walker[3]
Georgia Institute of Technology, Atlanta, GA, 30332, U.S.A

Alejandro Lopez Ortega[4]
Jet Propulsion Laboratory, California Institute of Technology, Pasadena, CA, 91109, U.S.A

Abstract: This paper presents a novel method of calibrating anomalous electron phenomena in fluid simulations of Hall thrusters. Specifically, this paper presents methods to calibrate the anomalous electron collision frequency, ν_{ea}, with measurements of the azimuthal electron drift velocity, $u_{e\theta}$, and to calibrate the anomalous electron heating, Q_{ea}, with measurements of the electron temperature, T_e. These methods are implemented in the Hall2De simulation code with incoherent laser Thomson scattering measurements of the axial profiles $u_{e\theta}$ and T_e along the channel centerline of a Hall thruster. Two primary simulations are considered, one that calibrates only ν_{ea} and another that simultaneously calibrates ν_{ea} and Q_{ea}. In addition, auxiliary simulations are calibrated using the uncertainty bounds of the measured $u_{e\theta}$ and T_e axial profiles that produce corresponding uncertainties in the axial profiles of ν_{ea} and Q_{ea}. We find that both primary simulations exhibit a sharp local minimum in ν_{ea} at the axial location corresponding to the maximum of $u_{e\theta}$. It is found that uncertainties in $u_{e\theta}$ produce large uncertainties in the downstream portion of the ν_{ea} profile. However, when only uncertainties in T_e are considered, there is a measurable difference in the ν_{ea} profiles between the two primary simulations. Lastly, while there is significant ambiguity in the calibrated profile of Q_{ea}, the calibrated profile shows significant deviation from the phenomenological model of Q_{ea} typically used in Hall thruster fluid simulations.

[1] Graduate Research Assistant, School of Aerospace Engineering, jlopezur3@gatech.edu
[2] Research Engineer, School of Aerospace Engineering
[3] Professor and William R. T. Oakes, Jr. School Chair, School of Aerospace Engineering, mitchell.walker@ae.gatech.edu
[4] Technologist, Electric Propulsion Group

I. Introduction

Hall effect thrusters (HETs) are the most common type of in-space propulsion [1]. However, the underlying physics behind HET operation is not understood well enough to enable fully predictive simulations with computational times required for design optimization. As a result, while HETs are widely used, costly experimental iterations on designs are still required to expand the operation envelope of HETs to different power levels or to alternative propellants. The lack of predictive capability in HET simulations has generally been attributed to anomalous electron transport across magnetic field lines, which is typically characterized by an anomalous electron collision frequency, ν_{ea}. This introduces a closure problem for simulations that treat electrons as a fluid, as these simulations need an equation for the ν_{ea} in terms of the other solution variables of the simulation. There have been several efforts to derive expressions for the ν_{ea} [2-7], but it is necessary to expand on previous experimental validation efforts [3,5,8-10].

The initial step in the validation of these theories typically starts by calibrating a HET simulation with experimental measurements to produce a semi-empirical spatial distribution of ν_{ea} [8,9,11]. Next, the plasma properties output by the simulation are combined with the theoretical closure to calculate a corresponding theoretical spatial distribution of ν_{ea}, which is compared with the semi-empirical distribution [2,3]. Alternatively, closure models can be implemented self-consistently within simulations, and the resultant simulation can be compared to a calibrated simulation [9,10]. Calibrated HET simulations [8,9,11] typically use laser-induced fluorescence (LIF) measurements of the axial ion velocity, u_{iz}, but experimental inferences of the electron Hall parameter or ν_{ea} can also be used [12-15]. However, incoherent laser Thomson scattering (ILTS) has measured peak electron temperatures significantly higher than those in calibrated simulations and Langmuir probe measurements [14,16,17]. This discrepancy has three important consequences. First, the calibrated profile of ν_{ea} should depend on the calibrated profile of the electron temperature, T_e, due to the electron pressure gradient, so accurately calibrated profiles of ν_{ea} require accurate profiles of T_e. Second, the theoretical closures may also depend on T_e, so validation of theoretical closures also requires accurate profiles of T_e. Third, these elevated electron temperatures introduce a second or third closure problem for anomalous electron heating, Q_{ea}, or for anomalous electron heat flux [15,18,19].

In this paper, we introduce a new way to calculate the anomalous electron collision frequency with an associated uncertainty that is based on combining ILTS measurements with Hall2De, a HET simulation software [20]. Specifically, we use ILTS measurements of the axial distributions of the azimuthal electron drift velocity, $u_{e\theta}$, and of T_e from Ref. 17. The measured $u_{e\theta}$ axial profile along the channel centerline is used to calibrate ν_{ea}, replacing the typical role of LIF measurements in calibrated simulations. The measured electron temperatures along the channel centerline are used to calibrate Q_{ea}. We chose to use a simulation instead of attempting to infer ν_{ea} directly from the measurements to minimize the assumptions used to infer the axial profile of ν_{ea} that corresponds to the ILTS measurements. Two primary simulations will be analyzed, one that only calibrates ν_{ea} and one that simultaneously calibrates ν_{ea} and Q_{ea}. Both calibrated simulations will be evaluated on their ability to reproduce the measured discharge current and the electron density profile measured by ILTS. The simulation that only calibrates ν_{ea} will also be evaluated on its ability to reproduce the electron temperature axial profile measured by ILTS. Section II describes the simulations and how the ILTS measurements are used to calibrate ν_{ea} and Q_{ea}. Section III presents the calibrated profiles of ν_{ea} and Q_{ea}, compares the two primary simulations, and discusses the implications of the findings for methods used to validate theories of ν_{ea} and Q_{ea}.

II. Methodology

A. Calibration Data

The ILTS measurements used for calibrating Hall2De in this work are taken from Ref. 17. The measurements were taken on the H9 HET at an operating condition of 171 V, 35 A, 87.5% of the nominal magnetic field strength, krypton as the propellant, and a background pressure of 1.2×10^{-5} Torr-Kr. The anode flow rate was 345 sccm, and the cathode flow rate was 23.7 sccm. A lower discharge voltage and the magnetic shielding of the H9 shift the acceleration downstream relative to nominal operating conditions on unshielded HETs, which in this particle case, shifted it entirely outside of the discharge channel. ILTS measurements have not been made inside the discharge channel of a HET, so the low discharge voltage enabled ILTS measurements across the acceleration region, which helps produce a more accurate calibrated simulation.

In interpolating the measurements, we omit certain points to smooth out the data input into Hall2De, as shown in Figs. 1 and 2. In addition, for $u_{e\theta}$, the data was also extrapolated upstream of the experimental domain. Such an extrapolation is qualitatively consistent with measurements of azimuthal electron current throughout the channel of a HET [21]. Lastly, to handle negative values of $u_{e\theta}$ appearing in the lower bounds of the inferences, we set a lower bound for $u_{e\theta}$ input values at 5 km/s.

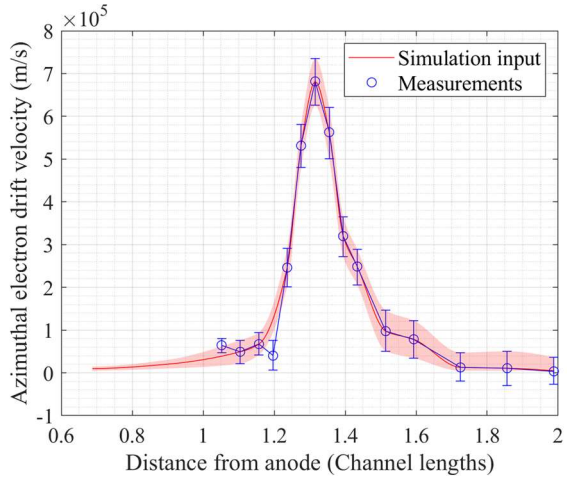

Figure 1. ILTS measurements and values used as Hall2De inputs of the azimuthal electron drift velocity. The boundaries of the shaded area were also used as Hall2De inputs. For the x-axis, 1 channel length corresponds to the channel exit plane.

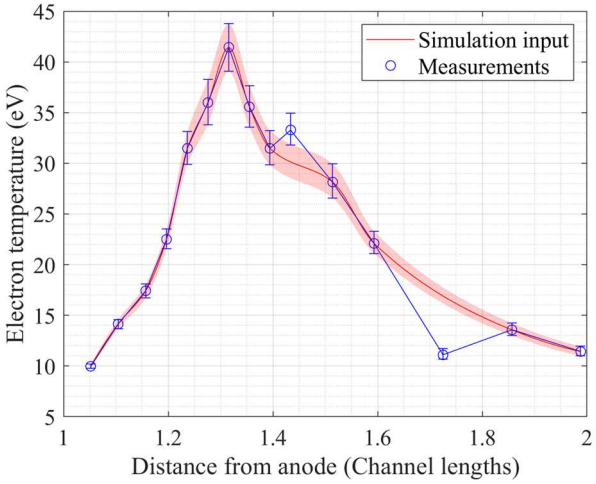

Figure 2. ILTS measurements and values used as Hall2De inputs of the electron temperature. The boundaries of the shaded area were also used as Hall2De inputs. For the x-axis, 1 channel length corresponds to the channel exit plane.

B. Hall2De

Hall2De is a 2-D radial-axial (axisymmetric) HET simulation code developed at the Jet Propulsion Laboratory [20]. Hall2De models the electrons as a fluid, and the version of Hall2De used in this work models the ions as a fluid and uses a line-of-sight algorithm to model the neutral dynamics [20]. In addition, Hall2De employs a

magnetic field-aligned mesh, which allows Hall2De to investigate plasma and erosion physics in environments with a complex magnetic field topology. As such, Hall2De has played an important role in the lifetime qualification of the AEPS thruster, XR-5, SPT-140, and MaSMi [22-25]. The simulation parameters other than the operating condition described are described in Table 1. One fluid corresponds to ions born above the discriminating potential (relative to the cathode exit), while the other fluid corresponds to ions born below the discriminating potential. The Sagdeev coefficient is used to for ν_{ea} in the cathode plume. In addition, to simulate the 171 V discharge voltage, we set the voltage difference between the anode and the cathode exit to 161 V [26]. We note that the discharge current is not specified because calibration with $u_{e\theta}$ provides the magnitude of ν_{ea}. This is in contrast with the calibrations done with the axial profile of u_{iz} that provide a normalized profile of ν_{ea} that is then scaled to match a specified discharge current [8]. For the simulations that only calibrate ν_{ea}, the timestep was set to 10 ns. When also calibrating for Q_{ea}, a timestep of 0.1 ns was used to prevent the simulation from immediately diverging.

Table 1. Simulation parameters

Parameter	Value
Number of ion fluids	2
Discriminating potential	50 V
Kr charge states	0,1,2,3
Sagdeev coefficient	10
Cathode ionization fraction	10 %
Cathode exit electron temperature	2 eV
Far field electron temperature	3 eV
Wall temperature	500 K

We ran one simulation that calibrates ν_{ea} with measurements of $u_{e\theta}$, and we ran another simulation that simultaneously calibrates ν_{ea} and Q_{ea} with measurements of $u_{e\theta}$ and the electron temperature. To quantify uncertainty in the results from the calibrated simulations, we ran auxiliary simulations that used the boundaries of the shaded areas in Figs. 1 and 2 as inputs for Hall2De. We consider the inferred results to be from simulations 1 and 4, and the error bounds for the results from simulation 1 are taken from simulations 1-3, while the error bounds for the results from simulation 4 are taken from simulations 4-6. In this manner, the reported uncertainty for simulation 4 only accounts for the uncertainty in the electron temperature measurements.

Table 2. Simulation inputs of the azimuthal electron drift velocities and electron temperatures from Figs. 1 and 2 used for each simulation. Lower bound and upper bound correspond to the lower and upper envelopes of the shaded regions in Figs. 1 and 2. Inference corresponds to the central curves within the shaded regions in Figs. 1 and 2.

Simulation	$u_{e\theta}$ input	T_e input
1	Inference	-
2	Lower bound	-
3	Upper bound	-
4	Inference	Inference
5	Inference	Lower bound
6	Inference	Upper bound

C. Anomalous Collision Frequency Closure

The typical closure problem considered is that of ν_{ea}. Once a closure for ν_{ea} is specified, then the cross-field and azimuthal electron momentum equations can be solved for the cross-field electron drift velocity, $u_{e\perp}$, and $u_{e\theta}$, assuming that all the other plasma properties are known. Neglecting electron inertia and assuming only singly-charged ions, the cross-field electron momentum equation is

$$E_\perp = u_{e\theta}B - \frac{\nabla_\perp(n_e T_e)}{n_e} - \frac{m_e \nu_e u_{e\perp}}{e} + \frac{m_e \nu_{ei} u_{i\perp}}{e} \tag{1}$$

where $\perp$ denotes the direction perpendicular to the magnetic field within the r-z plane, $\vec{E}$ is the electric field, $\vec{B}$ is the magnetic field, n_e is the electron density, m_e is the electron mass, e is the elementary charge, ν_e is the total electron collision frequency, ν_{ei} is the electron-ion momentum-transfer collision frequency, and $\vec{u}_i$ is the ion velocity vector. $\nu_e = \nu_{ec} + \nu_{ea}$, where ν_{ec} is the classical electron collision frequency. With the additional assumption of negligible ion azimuthal drift velocity, the axisymmetric azimuthal momentum equation can be written as

$$u_{e\theta} = -u_{e\perp}\Omega_e \tag{2}$$

where $\Omega_e = \frac{\omega_{ce}}{\nu_e}$ is the electron Hall parameter and ω_{ce} is the electron cyclotron frequency.

Given LTS measurements of $u_{e\theta}$, we iterate on the values of ν_{ea} until the values of $u_{e\theta}$ in Hall2De matches the measured values of $u_{e\theta}$, $u_{e\theta}^M$. Specifically, ν_{ea} along the channel centerline and within the experimental domain is iterated between timesteps i and $i+1$ using

$$\nu_{ea}^{i+1} = \nu_{ea}^{i} \exp\left[-a\left(1 - \frac{u_{e\theta}}{u_{e\theta}^M}\right)\right] \tag{3}$$

where $0 < a < 1$ is parameter that can be changed depending on the simulation to ensure stability of solution and reduce oscillations in the simulation. In this work, a was set between 0.001 and 0.01. Because the ILTS measurements are time-averaged, we are not concerned with simulating temporal dynamics. In Eq. 3, $u_{e\theta}$ is solved for using Eq. 2.

Outside the ILTS experimental domain, Eq. 2 is solved for $u_{e\theta}$, but a closure for ν_{ea} is needed. For the closure for ν_{ea}, we need to extrapolate values to downstream of the experimental domain, upstream of the experimental domain, and off-centerline. $\Omega_{ea} = \frac{\omega_{ce}}{\nu_{ea}}$ decreases significantly in the downstream portion of the experimental domain, so for the downstream extrapolation, we set Ω_{ea} as a constant and equal to the most downstream value of Ω_{ea} within the experimental domain. On the other hand, prior to the extrapolated values of $u_{e\theta}$ in Fig. 1, Ω_{ea} does not decrease sufficiently, which is why we chose to use extrapolated values of $u_{e\theta}$. Further upstream of the extrapolated experimental domain, we set Ω_{ea} as a constant and equal to the most upstream value of Ω_{ea} within the extrapolated experimental domain. Given that the measurements in Fig. 1 capture a large portion of the upstream increase in $u_{e\theta}$, we consider the upstream extrapolation method described above to be more accurate than setting the anomalous Hall parameter constant upstream of the experimental domain. Lastly, for the off-centerline values of ν_{ea}, we use the calculated values of ν_{ea} along the channel centerline and assume that Ω_{ea} is constant along magnetic field lines, an assumption that is commonly used in calibrated Hall2De simulations [8].

D. Anomalous Heating Closure

A closure for anomalous electron heating, Q_{ea}, has not received as much attention as a closure for ν_{ea} because fluid and hybrid HET simulations typically have fairly good agreement with Langmuir probe measurements of T_e,

particularly regarding the peak T_e along the channel centerline. However, recent ILTS measurements report peak electron temperatures around twice as high as typical Langmuir probe measurements [14,16,17]. While the exact source of this large discrepancy is unclear, the non-invasive nature and simpler analysis of ILTS measurements reduce the ambiguity of ILTS measurements compared to Langmuir probe measurements. As a result, we will use ILTS measurements of electron temperature to provide an experimental closure of Q_{ea}, but we acknowledge that the discrepancy between ILTS and Langmuir probes should be further investigated.

The experimental closure for anomalous electron heating presented below will ensure that Hall2De outputs the measured electron temperatures along the channel centerline. This serves two purposes. First, the electron pressure gradient is in the electron momentum equation, so its axial profile affects the resultant axial profile of ν_{ea} necessary to achieve a measured profile of $u_{e\theta}$. Consequently, an accurate axial profile of electron temperature is necessary to obtain an accurate axial profile of ν_{ea}. Second, this will provide an empirical profile of the anomalous electron heating that can be used to validate theoretical closures [27].

To calculate the values of Q_{ea} required to produce the measured electron temperatures, $T_{e,meas}$, along the channel centerline, we consider the electron energy equation,

$$\frac{3}{2}en_e\frac{\partial T_{eV}}{\partial t} = \vec{E}\cdot\vec{j}_e + \nabla\cdot\left(\frac{5}{2}T_{eV}\vec{j}_e - \vec{q}_e\right) - \frac{3}{2}T_{eV}\nabla\cdot\vec{j}_e - \sum_s \Phi_s + \mathrm{Q}_{el} + Q_{ea} \tag{4}$$

where $\vec{j}_e$ is the electron current density vector, $\vec{q}_e$ is the electron heat flux vector, Φ_s is inelastic energy loss of electrons from collisions with species s, and Q_{el} is rate of energy exchanged between electron and the heavy species due to thermal equilibration. Eq. 4 is discretized, and Q_{ea} is calculated such that the electron temperature in the next timestep $(i+1)$ is the measured electron temperature, using

$$Q_{ea} = \frac{3}{2}e[n_e]_i\frac{T_{e,meas}-[T_e]_i}{\Delta t} - \left[\vec{E}\cdot\vec{j}_e + \nabla\cdot\left(\frac{5}{2}T_{eV}\vec{j}_e - \vec{q}_e\right) - \frac{3}{2}T_{eV}\nabla\cdot\vec{j}_e - \sum_s \Phi_s + \mathrm{Q}_{el}\right]_i \tag{5}$$

where $[\,]_i$ denotes discretization or evaluation at the i^{th} timestep. The Q_{ea} calculated with Eq. 5 is then used in the discretized form of the electron energy equation used in Hall2De.

However, it is important to note that Eq. 4 typically includes a phenomenological formulation of anomalous electron heating through the Joule heating term, $\vec{E}\cdot\vec{j}_e$. To illustrate this, we consider the instantaneous Ohm's Law and neglect the electron pressure gradient without loss of generality,

$$\vec{E} \approx \vec{u}_e \times \vec{B} + \eta_c\vec{j}_e \tag{6}$$

where we use the classical electron resistivity, η_c, because anomalous effects are predominantly time-averaged effects. Then, the instantaneous $\vec{E}\cdot\vec{j}_e$ is given by

$$\vec{E}\cdot\vec{j}_e = \eta_c j_e^2 \,. \tag{7}$$

However, in radial-axial fluid or hybrid simulations like Hall2De, $\vec{E}\cdot\vec{j}_e$ is not computed as the full three-dimensional dot product, but as $\left(\vec{E}\cdot\vec{j}_e\right)_{rz} = E_\perp j_{e\perp} + E_\parallel j_{e\parallel}$. Using the instantaneous Ohm's law,

$$\left(\vec{E}\cdot\vec{j}_e\right)_{rz} = j_{e\perp}u_{e\theta}B + \eta_c\left(j_{e\perp}^2 + j_{e\parallel}^2\right) \tag{8}$$

which includes a non-zero magnetic work term. Using Eq. 2, we can rewrite $j_{e\perp}u_{e\theta}B = (\eta_c + \eta_a)j_{e\theta}^2$ such that

$$\left(\vec{E}\cdot\vec{j}_e\right)_{rz} = \eta_c j_e^2 + \eta_a j_{e\theta}^2 \,. \tag{9}$$

As a result, axial-radial fluid simulations typically include a phenomenological anomalous electron heating term of $Q_{ea} = \eta_a j_{e\theta}^2$, which is the dominant term in $\vec{E}\cdot\vec{j}_e$. Hall2De also has an additional heating term of $\eta_a j_{e\perp}^2$ for a total phenomenological anomalous electron heating of $Q_{ea} = \eta_a(j_{e\theta}^2 + j_{e\perp}^2)$. We are interested in calculating the true anomalous electron heating, not just that in addition to a phenomenological term, so we use $\vec{E}\cdot\vec{j}_e = \left(\vec{E}\cdot\vec{j}_e\right)_{rz} - \eta_a(j_{e\theta}^2 + j_{e\perp}^2)$ when calculating the Joule heating term in Eq. 5. We also note that because HET simulations have historically used this phenomenological heating term that has little physical basis, the fact that Langmuir probe measurements of electron temperature agree well with simulations has reduced significance. However, we note that a recent theory for Q_{ea} suggests that Q_{ea} is proportional to $\eta_a j_{e\theta}^2$ [27], so $\eta_a j_{e\theta}^2$ or $\eta_a(j_{e\theta}^2 + j_{e\perp}^2)$ can be used as reference values for Q_{ea}.

Regarding the physical origin of Q_{ea}, the above formulation of $\vec{E}\cdot\vec{j}_e + Q_{ea}$ is consistent with treating Q_{ea} as the result of correlated azimuthal fluctuations of $\vec{E}$ and $\vec{j}_e$. Specifically, we can write the azimuthally averaged Joule heating as

$$\vec{E}\cdot\vec{j}_e = \left(\vec{E}\cdot\vec{j}_e\right)_{rz} + \langle E_\theta j_{e\theta}\rangle_\theta \tag{10}$$

where $\langle E_\theta j_{e\theta}\rangle_\theta$ is the azimuthal correlation of azimuthal fluctuations in E_θ and $j_{e\theta}$. $\langle E_\theta j_{e\theta}\rangle_\theta$ can be decomposed into $-e\langle u_{e\theta}\rangle_\theta\langle\delta E_\theta\delta n_e\rangle_\theta - e\langle n_e\rangle_\theta\langle\delta E_\theta\delta u_{e\theta}\rangle_\theta - e\langle\delta E_\theta\delta n_e\delta u_{e\theta}\rangle_\theta$, where $\langle\,\rangle_\theta$ denotes the azimuthal average of a property and δ denotes the deviation of a property from its azimuthal average. In addition, it is well understood that correlated azimuthal fluctuations are the predominant cause of ν_{ea} [2,3], such that $\langle E_\theta\delta n_e\rangle_\theta = -\eta_a n_e j_{e\theta}$. The azimuthally averaged Joule heating can then be written as

$$\vec{E}\cdot\vec{j}_e = \left(\vec{E}\cdot\vec{j}_e\right)_{rz} - \eta_a j_{e\theta}^2 - e n_e\langle\delta E_\theta\delta u_{e\theta}\rangle_\theta - e\langle\delta E_\theta\delta n_e\delta u_{e\theta}\rangle_\theta \tag{11}$$

Therefore, the formulation of Q_{ea} used in this work corresponds to the definition of $Q_{ea} = -e n_e\langle\delta E_\theta\delta u_{e\theta}\rangle_\theta - e\langle\delta E_\theta\delta n_e\delta u_{e\theta}\rangle_\theta$.

To calculate Q_{ea} outside of the experimental domain, we use analogous extrapolation methods to those used for ν_{ea}. For the downstream extrapolation, we set $\frac{Q_{ea}}{\eta_a(j_{e\theta}^2+j_{e\perp}^2)}$ as a constant and equal to the most downstream value of $\frac{Q_{ea}}{\eta_a(j_{e\theta}^2+j_{e\perp}^2)}$ in the experimental domain. For the upstream extrapolation, we set $\frac{Q_{ea}}{\eta_a(j_{e\theta}^2+j_{e\perp}^2)}$ as a constant and equal to the most upstream value of $\frac{Q_{ea}}{\eta_a(j_{e\theta}^2+j_{e\perp}^2)}$ in the experimental domain. For the off-centerline extrapolation, we assume that $\frac{Q_{ea}}{\eta_a(j_{e\theta}^2+j_{e\perp}^2)}$ is constant along magnetic field lines.

Lastly, similar to how the pressure gradient affects the calculated ν_{ea}, the divergence of the electron heat flux, $\vec{q}_e$, affects the calculated Q_{ea}. In addition, ILTS measurements of non-isothermal field lines indicate that the typical conductive electron heat fluxes used in HET fluid simulations may need to be modified [19,28,29]. However, in the absence of a known closure for the heat fluxes parallel and perpendicular to the magnetic field, we will still use the typical electron heat fluxes used in Hall2De. Therefore, there will be significant ambiguity in the presented values of Q_{ea} and future work will investigate how the calibrated Q_{ea} axial profile depends on the heat flux closure.

III. Results and Discussion

In this section, we present, evaluate, and compare the results of two primary simulations, one calibrated on only ν_{ea} and another calibrated on both ν_{ea} and Q_{ea}. Specifically, we start by comparing the profiles of ν_{ea} of both simulations and present the calibrated profile of Q_{ea}. For both simulations, we compare the calibrated axial profiles of electron density and the calibrated discharge current with measured values. For the simulation that only calibrates ν_{ea}, we also compare the calibrated electron temperature axial profile to measured values.

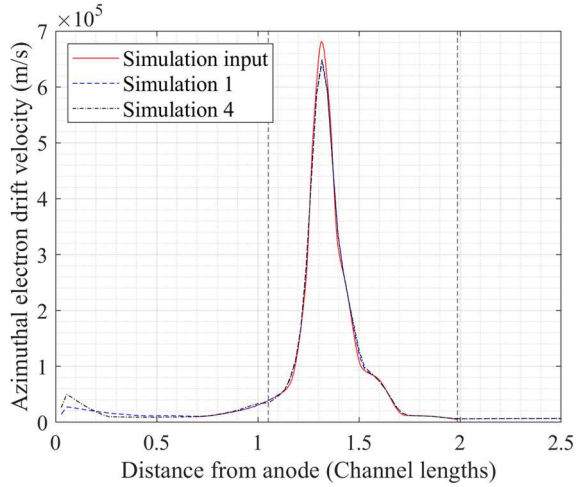

Figure 3. Axial profile of azimuthal electron drift velocity along the channel centerline for the same simulation input of simulations 1 and 4 and for the results of simulations 1 and 4 without their corresponding uncertainty. Vertical dashed lines denote the experimental domain.

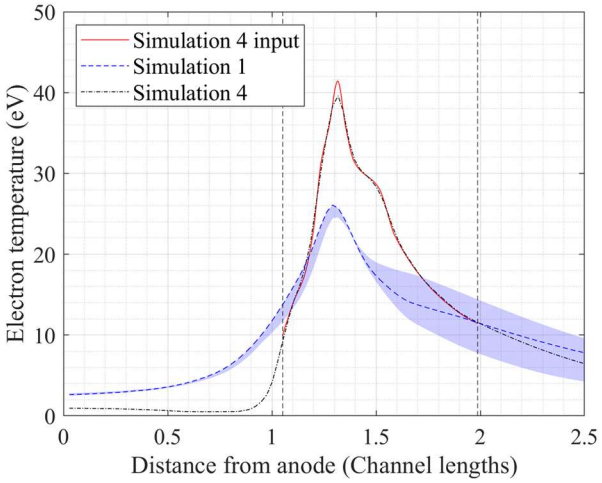

Figure 4. Axial profile of electron temperature along the channel centerline for the simulation 4 input, simulation 1 with uncertainty, and simulation 4 without uncertainty. Vertical dashed lines denote the experimental domain.

Figures 3 and 4 confirm that the calibrated simulations match the input values for $u_{e\theta}$ and T_e and also show how $u_{e\theta}$ and T_e vary outside of the experimental domain. Figure 4 also shows that peak electron temperature measured with ILTS is around 50% higher than that predicted by the simulations that only calibrate ν_{ea}. However, elsewhere in the axial profile, the simulations predict electron temperatures higher than the measured values; while this could be attributed to an inaccurate model of the electron heat flux, it could also be caused by an axial variation in $\frac{Q_{ea}}{\eta_a(j_{e\theta}^2+j_{e\perp}^2)}$. In addition, the peak electron temperatures of simulations 1-3 are around 15% of the discharge voltage, similar to what has typically been found in fluid simulations and Langmuir probe measurements of magnetically shielded HETs [30]. While the discrepancy between HET simulations and ILTS measurements can be explained by alternative models of anomalous electron heating, further investigation is needed to determine whether the discrepancy between ILTS and Langmuir probes are due to perturbation of the discharge, inaccurate sheath models used in the analysis of Langmuir probe measurements, or another phenomenon. For example, while simultaneous LIF and Langmuir probe measurements have shown perturbation of a HET discharge by a Langmuir probe, simultaneous ILTS and Langmuir probe measurements should be carried out to determine if perturbations alone can explain the discrepancy in electron temperature measurements. Furthermore, Ref. [31] showed that an alternative analysis of raw Langmuir probe

measurements can result in electron temperature measurements similar to those of ILTS, but the validity of such an analysis needs to be investigated.

Fig. 5 demonstrates that the calibrated profiles of ν_{ea} of both primary simulations exhibit a sharp local minimum in ν_{ea} in the acceleration region. This is in contrast with previous suggestions that high electron temperatures could suppress the sharp local minimum in ν_{ea} [14,19]. Interestingly, simulation 4 that calibrates Q_{ea} has a sharper local minimum in ν_{ea} than simulation 1. In addition, the profile of ν_{ea} for simulation 1 exhibits large uncertainty further downstream, which is attributed to the simulation that uses the upper bound of the $u_{e\theta}$ measurements. Even in the regions with lower uncertainty in ν_{ea}, the error bounds of calibrated profiles of ν_{ea} overlap for the two simulations, indicating no significant change in ν_{ea} between the simulations. However, the measured peak electron temperature is only 50% higher than that predicted by simulation 1, so it is possible that other discharge conditions where this difference is larger could have significant deviations in ν_{ea} depending on whether Q_{ea} is calibrated. It is interesting to note that calibrated ν_{ea} profiles from LIF measurements exhibit large uncertainties in the upstream portion of the profile [8,32], while ν_{ea} from ILTS measurements exhibit large uncertainties in the downstream portion of the profile. This suggests that, if used together, LIF and ILTS measurements could provide low uncertainty calibrated profiles of ν_{ea}, provided that ILTS measurements can access the upstream portion of the acceleration region.

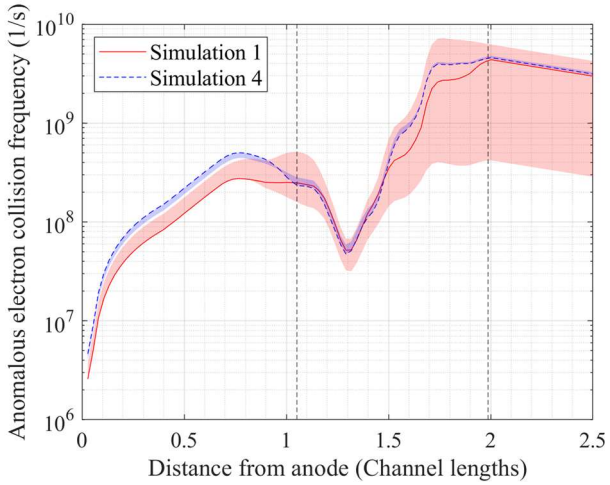

Figure 5. Axial profile of the anomalous electron collision frequency along the channel centerline for simulations 1 and 4 with all their associated uncertainty. Vertical dashed lines denote the experimental domain.

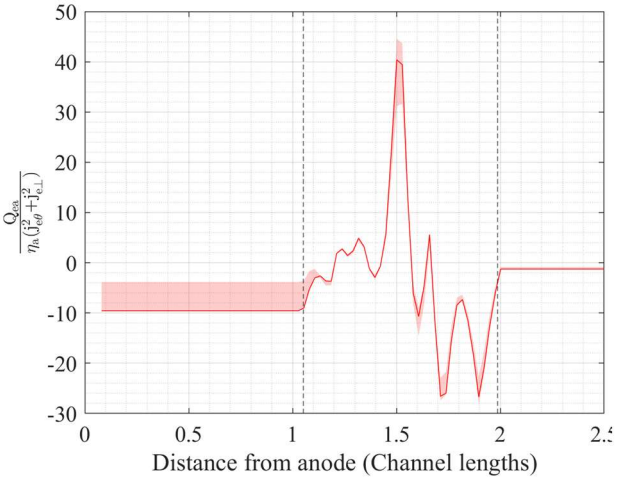

Figure 6. Axial profile along the channel centerline of $\frac{Q_{ea}}{\eta_a(j_{e\theta}^2+j_{e\perp}^2)}$ for simulation 4 with the corresponding uncertainty. Vertical dashed lines denote the experimental domain.

Another way of evaluating the significance of calibrating Q_{ea} on the profile of ν_{ea} is to compare simulations 1 and 4 without accounting for the uncertainty in $u_{e\theta}$. Figure 5 demonstrates that if only the uncertainty due to electron temperature measurements is accounted for, then there is a measurable difference in the axial profile of ν_{ea}, depending on whether Q_{ea} is calibrated. Consequently, if low uncertainty inferences of ν_{ea} are possible, then a simultaneous calibration of Q_{ea} is required for an accurate profile of ν_{ea}. Therefore, when validating theories of anomalous electron

transport with calibrated profiles ν_{ea}, it may be important to ensure that the calibrated simulation also has accurate calibrated electron temperatures.

The calibrated profile of $\frac{Q_{ea}}{\eta_a(j_{e\theta}^2+j_{e\perp}^2)}$ shows a few interesting features. For reference, we note that when Q_{ea} is not calibrated, $\frac{Q_{ea}}{\eta_a(j_{e\theta}^2+j_{e\perp}^2)}=1$. First and unsurprisingly, $\frac{Q_{ea}}{\eta_a(j_{e\theta}^2+j_{e\perp}^2)}$ has a local maximum at the location of the peak electron temperature. Second, at this local maximum, $\frac{Q_{ea}}{\eta_a(j_{e\theta}^2+j_{e\perp}^2)}$ is around 4.5, which reflects the fact that simulation 1 underpredicts the peak electron temperature with respect to the ILTS measurements. Third, the largest peak occurs at an axial location of 1.5 channel lengths from the anode, which in Fig. 4 corresponds to where the slope of the electron temperature profile briefly increases while T_e is decreasing. Interestingly, Q_{ea} is negative for a significant portion of the profile. However, we reiterate that the ambiguity of the correct electron heat flux model creates significant ambiguity in the presented profile of $\frac{Q_{ea}}{\eta_a(j_{e\theta}^2+j_{e\perp}^2)}$. In addition, due to isothermal field lines, the profile of Q_{ea} along the channel centerline depends on the extrapolation of Q_{ea} along the field lines. Therefore, the ambiguity of how Q_{ea} varies along magnetic field lines further increases the ambiguity in the profile presented in Fig. 6. To gain insight into the spatial distribution of Q_{ea}, kinetic simulations of HETs should calculate the Q_{ea} produced by correlations of turbulent fluctuations, similar to what has been done for ν_{ea} [33].

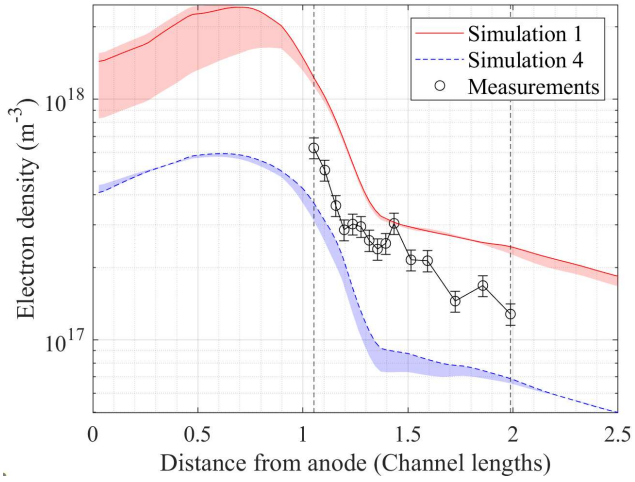

Figure 7. Axial profile of electron density along the channel centerline for simulations 1 and 4 with corresponding uncertainty and for ILTS measurements. Vertical dashed lines denote the experimental domain.

Table 3 shows that the simulation that only calibrates ν_{ea} results in a calibrated discharge current significantly closer to the measured value than the simulation that calibrates both ν_{ea} and Q_{ea}. Specifically, simulation 1 has a calibrated discharge current of 30.0 + 2.7 / - 5.7 A, and simulation 4 has a calibrated discharge current of 8.7 + 0.3 / - 0.7 A. However, because the discharge current is predominantly the thermal electron flux through the anode sheath, the discharge current depends on the electron density and temperature near the anode, which in turn depends on the methods used to extrapolate ν_{ea} and Q_{ea} upstream of the experimental domain. It can be seen in Fig. 4 that the

upstream extrapolation of Q_{ea} results in a noticeable difference in the upstream electron temperature between simulations 1 and 4, which partially explains the lower discharge current for simulation 4. In addition, the discharge current also depends on the values of the electron density and temperature off centerline, so the discharge current should also depend on the extrapolation of ν_{ea} and Q_{ea} along magnetic field lines. Therefore, because the methods used to extrapolate ν_{ea} and Q_{ea} have not been validated, the calibrated values of discharge current have some ambiguity and may not be the best way to evaluate the calibrated simulations.

Table 3. Calibrated discharge current of each simulation

Simulation	Discharge current (A)
1	30.0
2	32.7
3	24.3
4	8.7
5	8.0
6	9.0

However, evaluating the calibrated simulations with the calibrated axial profiles of the electron density is also ambiguous. Figure 7 shows that simulation 1 overpredicts the electron density with respect to ILTS measurements, while simulation 4 underpredicts the electron density. While simulation 4 converged, we observed that as the discharge current dropped, so did the electron density, which is expected. However, this indicates that the inaccuracies in the extrapolations of ν_{ea} and Q_{ea} to outside the experimental domain also affect the calibrated axial profile of the electron density. Therefore, to enable accurate independent validations of calibrated simulations via comparison with the measured discharge current or electron density profile, accurate extrapolations of ν_{ea} and Q_{ea} are needed upstream and downstream of the experimental domain and along magnetic field lines.

IV. Conclusion

Simultaneous calibration of ν_{ea} and Q_{ea} demonstrates that while the higher electron temperatures measured by ILTS do not significantly alter the general characteristics of the axial profile of ν_{ea}, if low uncertainty inferences of ν_{ea} are made, then an accurate electron temperature profile is necessary to ensure an accurate inference of ν_{ea}. This adds some ambiguity to the validations of theories of ν_{ea} with calibrated simulations that do not produce an accurate axial profile of electron temperature. In addition, the regions with the highest uncertainty in the profile of ν_{ea} when calibrated within $u_{e\theta}$ suggest that ILTS and LIF can be combined to produce profiles of ν_{ea} with relatively low uncertainty throughout the acceleration region. While we have produced a calibrated profile of Q_{ea} that shows a significant deviation from the phenomenological model of Q_{ea}, future work is planned for evaluating how this calibrated profile depends on the electron heat flux model. Regarding the evaluation of the calibrated simulation with independent measurements of the discharge current and electron density, these evaluations are strongly dependent on the unvalidated extrapolations of ν_{ea} and Q_{ea} to outside the experimental domain. As a result, improvement of the extrapolation methods is essential to increasing the accuracy of the calibrated simulations.

Acknowledgments

Funding for this work was provided through NASA Space Technology Graduate Research Opportunity grant 80NSSC23K1217. Part of this research was carried out at the Jet Propulsion Laboratory, California Institute of Technology, under a contract with the National Aeronautics and Space Administration (80NM0018D0004). The authors also thank Yiangos Mikellides for insightful discussions.

References

[1] Tirila V.-G., Demaire A., Ryan C. N., "Review of alternative propellants in Hall thrusters," Acta Astronautica 212, 284-306, 2023.

[2] Lafleur T., Baalrud S. D., Chabert P., "Theory for the anomalous electron transport in Hall effect thrusters. II. Kinetic model," Physics of Plasmas 23, 053503, 2016.

[3] Mikellides I. G., Lopez Ortega A., Chaplin V. H., "Theory of the anomalous momentum exchange from wave-particle interactions in Hall-effect ion accelerators and comparisons with measurements," Physics of Fluids 36, 074121, 2024.

[4] Cappelli M. A., Young C. V., Cha E., Fernandez E., "A zero-equation turbulence model for two-dimensional hybrid Hall thruster simulations," Physics of Plasmas 22, 114505, 2015.

[5] Jorns B., "Predictive, data-driven model for the anomalous electron collision frequency in a Hall effect thruster," Plasma Sources Science and Technology 27, 104007, 2018.

[6] Katz I., Mikellides I. G., Jorns B. A., Lopez Ortega A., "Hall2De simulations with an anomalous transport model based on the electron cyclotron drift instability," 34th International Electric Propulsion Conference, IEPC-2015-402, 2015.

[7] Jorns B. A., "Two equation closure model for plasma turbulence in a Hall effect thruster," 36th International Electric Propulsion Conference, IEPC-2019-129, 2019.

[8] Mikellides I. G., Lopez Ortega A., "Challenges in the development and verification of first-principles models in Hall-effect thruster simulations that are based on anomalous resistivity and generalized Ohm's law," Plasma Sources Science and Technology 28, 014003, 2019.

[9] Marks T. A., Jorns B. A, "Evaluation of algebraic models of anomalous transport in a multi-fluid Hall thruster code," Journal of Applied Physics 134, 153301, 2023.

[10] Marks T. A., Jorns B. A., "Challenges with the self-consistent implementation of closure models for anomalous electron transport in fluid simulations of Hall thrusters," Plasma Sources Science and Technology 32, 045016, 2023.

[11] Garrigues L., Perez-Luna J., Lo J., Hagelaar J. M., Boeuf J. P., Mazouffre S., "Empirical electron cross-field mobility in a Hall effect thruster," Applied Physics Letters 95, 141501, 2009.

[12] Linnel J. A., Gallimore A. D., "Hall thruster electron motion characterization based on internal probe measurements," 31st International Electric Propulsion Conference, IEPC-2009-105, 2009.

[13] Dale E. T., Jorns B. A., "Non-invasive time-resolved measurements of anomalous collision frequency in a Hall thruster," Physics of Plasmas 26, 013516, 2019.

[14] Roberts P. J., Jorns B. A., "Laser measurement of anomalous electron diffusion in a crossed-field plasma," Physical Review Letters 132, 135301, 2024.

[15] Brick D. G., Jorns B. A., "Model based investigation of anomalous energy transport in a magnetically-shielded Hall thruster," 38th International Electric Propulsion Conference, IEPC-2024-411, 2024.

[16] Vincent B., Tsikata S., Mazouffre S., "Incoherent Thomson scattering measurements of electron properties in a conventional and magnetically-shielded Hall thruster," Plasma Sources Science and Technology 29, 035015, 2020.

[17] Lopez-Uricoechea J., Suazo Betancourt J. L., Butler-Craig N., Walker M. L. R., "Spatially resolved Thomson scattering measurements of electron properties across the acceleration region of a high-power magnetically shielded Hall effect thruster," Journal of Applied Physics 136, 113303, 2024.

[18] Roberts P. J., Jorns B., "Inferring electron heat flux in a high-power Hall thruster with incoherent Thomson scattering," AIAA SCITECH 2024 Forum, AIAA-2024-1957, 2024.

[19] Brick D. G., Roberts P. J., Jorns B., "Numerical investigation of electron energy transport in Hall thrusters," AIAA SCITECH 2025 Forum, AIAA-2025-0298, 2025.

[20] Mikellides I. G., Katz I., "Numerical simulations of Hall-effect plasma accelerators on a magnetic-field-aligned mesh," Physical Review E 86, 046703.

[21] Mullins C. R., Farnell C. C., Farnell C. C., Martinez R. A., Liu D., Branam R. D., Williams J. D., "Non-invasive Hall current distribution measurement in a Hall effect thruster," Review of Scientific Instruments 88, 013507, 2017.

[22] Hofer R., Lobbia R., Chaplin V., Lopez Ortega A., Mikellides I., et al. "Completing the Development of the 12.5 kW Hall Effect Rocket with Magnetic Shielding (HERMeS)," International Electric Propulsion Conference, IEPC-2019-193, 2019.

[23] Lopez Ortega A., Jorns B. A., Mikellides I. G., Hofer R. R., "Numerical simulations of the XR-5 Hall thruster for life assessment at different operating conditions," 51st AIAA Joint Propulsion Conference, AIAA 2015-4008, 2015.

[24] Lopez Ortega A., Mikellides I. G., Chaplin V. H., Snyder J. S., Lenguito G., "Numerical Investigations of Background Pressure Effects and Channel Erosion in the SPT-140 Hall thruster for the Psyche Mission," International Electric Propulsion Conference, IEPC 2019-263, 2019.

[25] Conversano R. W., Barchowsky A., Lobbia R. B., et al., "Overview of the Ascendant Sub-kW Transcelestial Electric Propulsion System (ASTRAEUS)." International Electric Propulsion Conference, IEPC-2019-282, 2019.

[26] Lopez Ortega A., Mikellides I. G., "The importance of the cathode plume and its interactions with the ion beam in numerical simulations of Hall thrusters," Physics of Plasmas 23, 043515, 2016.

[27] Mikellides I. G., Lopez Ortega A., "First-principles model for the anomalous frictional heating of electrons in Hall thrusters," AIAA SCITECH Forum, AIAA-2025-0294, 2025.

[28] Suazo Betancourt J. L., Butler-Craig N., Lopez-Uricoechea J., Steinberg A. M., Walker M. L. R., "Laser Thomson scattering measurements indicate non-isothermal magnetic field lines in magnetically shielded Hall effect thrusters," Physics of Plasmas 31, 113106, 2024.

[29] Roberts P. J., Allen M. G., Brick D. G., Jorns B. A., "Empirical closures for momentum and energy transport in Hall thrusters based on Thomson scattering measurements," 38th International Electric Propulsion Conference, IEPC-2024-393, 2024.

[30] Mikellides I. G., Katz I., Hofer R. R., Goebel D. M., "Magnetic shielding of a laboratory Hall thruster. I. Theory and validation," Journal of Applied Physics 115, 043303, 2014.

[31] Roberts P., "Characterization of momentum and heat flow in Hall thrusters with laser scattering," Ph. D. dissertation (University of Michigan, 2025).

[32] Lopez Ortega A., Mikellides I. G., "Erosion mechanisms at the outer front pole cover of a magnetically shielded Hall thruster," 38th International Electric Propulsion Conference, IEPC-2024-264, 2024.

[33] Adam J. C., Boeuf J. P., Dubuit N., Dudeck M., Garrigues L., et al., "Physics, simulation and diagnostics of Hall effect thrusters," Plasma Physics and Controlled Fusion 50, 124041, 2008.